sustainability

MDPI

Article

Fractional Vegetation Cover Estimation of Different Vegetation Types in the Qaidam Basin

Siqi Zhang, Hui Chen *, Yang Fu, Huihui Niu, Yi Yang and Boxiong Zhang

Hebei Key Laboratory of Environmental Change and Ecological Construction, College of Resources and Environment Sciences, Hebei Normal University, Shijiazhuang 050024, China; zhangsq0511@163.com (S.Z.); young1dk1@163.com (Y.F.); niuhuihui17@163.com (H.N.); yangyi956@163.com (Y.Y.); zbx1039841440@126.com (B.Z.)

* Correspondence: chenhui@igsnrr.ac.cn; Tel.: +86-0311-8078-7625

Received: 20 December 2018; Accepted: 1 February 2019; Published: 7 February 2019

check for updates

Abstract: The estimation of fractional vegetation cover (FVC) by using remote sensing images has become feasible. Based on Landsat8-OLI images and field data obtained from an unmanned aerial vehicle, we established an empirical model (EM) and a pixel decomposition model (PDM) of FVC in the desert vegetation region, steppe vegetation region, meadow vegetation region and mixed vegetation region (the three vegetation region types) of the Qaidam Basin, and the inversion accuracies of the models were compared. The results show the following: (1) Vegetation classification inversion (VCI) provides a promising approach for FVC estimation. The accuracy of FVC by VCI was obviously better than that achieved using vegetation mixed inversion (VMI); (2) Differences were observed in the FVC estimation between VCI and VMI by the EM in areas with relatively high-density vegetation cover (FVC > 60%). The FVC in some parts of steppe region in the basin was slightly overestimated by VMI of the EM; 3) VCI estimated by the PDM resulted in lower inversion values for extremely low-density vegetation cover (FVC $\leq$ 10%) and higher inversion values for high-density vegetation cover (FVC > 80%). The FVC inversion was underestimated by the PDM in steppe and meadow regions with FVC > 15% in the basin. The application of VCI in different models can provide new ideas for the sustainable study of vegetation in arid regions.

Keywords: fractional vegetation cover; empirical model; pixel decomposition model; accuracy evaluation

1. Introduction

Vegetation is a vital part of ecosystems and provides a link among the soil, atmosphere and moisture. It plays an important role in the energy exchange of the land surface, the global biochemical cycle and the water cycle [1,2]. Fractional vegetation cover (FVC) is defined as the projected percentage of the total study area that is vegetated (roots, stems and leaves) [3]. FVC not only reflects the size of the plant photosynthetic area and the density of vegetation growth but also represents the growth trend of vegetation to some extent [4,5]. As an important parameter for the balance and development of terrestrial ecosystems, FVC is widely used in related research on climate change, soil and hydrology [6–9].

The development of remote sensing technology has provided a promising tool for FVC estimation [10,11]. There are several methods applied to the FVC inversion via remote sensing, including the empirical model (EM) [12], the pixel decomposition model (PDM) [13], the artificial neural networks [14], the decision tree classification [15,16], and the physical model [17]. In particular, EM and PDM are used as basic approaches in most FVC studies based on remote sensing data [18,19].

The EM estimates the FVC based on the regression relationship between the measured data and vegetation index (VI, different band information combination of images, indicating vegetation growth status) [20], such as the normalized difference vegetation index (NDVI) or the ratio vegetation index (RVI), to invert the FVC [21,22]. For instance, Voorde [23] reported that an EM constructed by band could produce sufficient accuracy in estimating the FVC of trees in Brussels. However, some research has shown that the EM is susceptible to vegetation type and the quality and quantity of measured data, that is, this strategy provides ideal results in homogeneous areas at regional scales (e.g., simple steppe regions or forest regions) [12,24,25]. Furthermore, it is still not clear how to extend the scope of an EM in relatively complex regions with multiple vegetation types [26–28].

The PDM is a method that decomposes the vegetation information of image pixels to indirectly estimate the FVC [29]. This approach with fixed or variable endmembers has been widely used in regional to global scale studies [30–32]. The majority of PDM modeling applications are restricted to two (vegetation and non-vegetation), three (green vegetation, non-photosynthetic vegetation and bare soil) or four endmembers (green vegetation, non-photosynthetic vegetation, bare soil and shadow) by the methods of Count-Based endmember selection or Minimum Average Spectral angle, etc. [33,34]. Because of the PDM of two endmembers simplify the endmember selection process, it improves efficiency and application substantially with relatively high precision [35].

However, the PDM of two endmembers assumed to the spectral variability within an endmember negligible, still remain disputes about the accuracy of the model because of the choice of endmember threshold [35–38]. Several studies have attempted to improve the accuracy of models by setting a fixed threshold based on higher precision remote sensing images or using different VIs [35,39]. The estimation results of these approaches usually vary greatly depending on the regions or vegetation types. As a result, there exist significant differences in inversion details of FVC for different density areas by different methods of endmember extraction. To our knowledge, the simplification of endmember information based on different vegetation types has not been seriously considered.

The Qaidam Basin, located on the northern Qinghai-Tibet Plateau, is one of the most sensitive areas to global climate change [40]. The basin is a typical arid ecosystem with a fragile ecological environment, and it is an ideal area in which to study FVC under natural conditions due to relatively few proximate human activities. However, most research focused on the relationship between FVC and climate factors in alpine steppe-meadow of Qinghai-Tibet Plateau or the study of vegetation of arid areas [7,11,41]. FVC estimation methods and detailed features of different vegetation types within the basin were often ignored. In addition, the complex topography and the diversity of vegetation in the basin produce strong spatial variation in FVC. Traditional methods of employing FVC inversion using EM and PDM pose a challenge to estimating FVC accurately in the complex basin [33]. Thus, improving the accuracy and applicability of an EM and a PDM in this complicated area is an urgent task that can provide guidance for the estimation of FVC in other regions.

In this study, we acquired a large amount of surface-measured data by using a digital camera mounted on an unmanned aerial vehicle (UAV) combined with vegetation type distribution data and remote sensing images from Landsat8-OLI. The inversion accuracy of the EM and PDM in measuring the FVC of desert, steppe, meadow and mixed vegetation regions of the basin were verified by comparative analysis. Our objective is to understand the inversion details of different models under different vegetation types and to develop a suitable method for improving the accuracy and applicability of FVC estimation in complicated arid regions. In addition, the accuracy of FVC distribution from the measured data at the quadrat scale to the large scale in the Qaidam Basin was investigated.

2. Study Area

The Qaidam Basin, located on the northern part of the Qinghai-Tibet Plateau, northwest of Qinghai Province in China, is a closed tectonic basin surrounded by the Altun Mountains, Kunlun Mountains and Qilian Mountains. The basin is divided into two parts, including arid desert area inside the basin and alpine area around the basin. The inner elevation is 2652–3350 m and the annual precipitation is 15–200 mm in the basin. The around the basin is cold with an altitude of 3560–6860 m. The basin has a typical plateau continental climate with low rainfall and high evaporation [42]. Rivers and lakes such as Gasikule Lake, Hala Lake and Golmud River are widely distributed in the basin (Figure 1). The biogeographical province of the Qaidam Basin belongs to "Takal-Makan-Gobi Desert of the Palaearctic Realm" and its characteristic biome is in the group "Cold-winter (continental) deserts and semi deserts" [43]. The vegetation in the Qaidam Basin is relatively sparse with simple plant communities. According to the characteristics of composition, appearance and structure of vegetation communities, there are nine types of vegetation communities in the basin according to the Chinese vegetation classification, such as desert communities (e.g., *Ceratoides latens* and *Nitraria tangutorum*), steppe communities (e.g., *Stipa purpurea* and *Achnatherum splendens*), meadow communities (e.g., *Kobresia tibetica* and *Phragmites australis*) and forest communities (e.g., *Sabina chinensis*). Desert, steppe and meadow communities are the main types of vegetation in the basin. In this paper, we investigated and photographed many communities such as *Ceratoides latens* desert, *Haloxylon ammodendron* desert, *Stipa purpurea* steppe, *Kobresia humilis* meadow, etc.

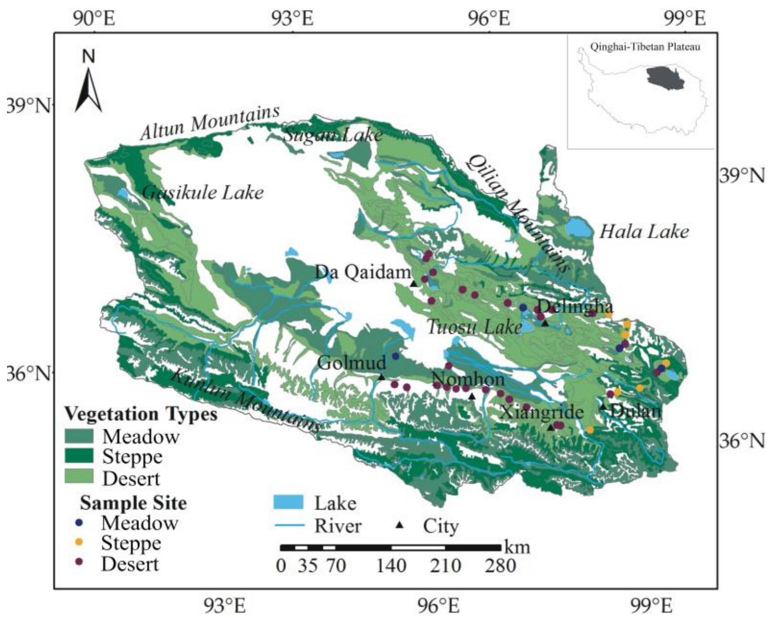

Figure 1. Distribution of vegetation and the sample site in the Qaidam Basin.

3. Data and Methods

3.1. Data Source and Preprocessing

Ground-measured data were obtained by taking pictures in the field with a UAV platform named Phantom 3 Advance. The hovering accuracy of UAV was ±1.5 m horizontally and ±0.5 m vertically with the ability of vertical take-off and landing. Therefore, it can hover and shoot steadily. The UVA equipped with a 4k ultra clear digital camera containing three channels of red, green and blue. We randomly selected areas covered with vegetation in the central and eastern desert, steppe and meadow regions of the basin as the sample sites (Figure 1), with a total of 39 sample sites (200 m × 200 m). To provide comprehensive and detailed information of FVC for each site, we set the route to shoot 16 images at each site (Figure 2). Thus, each site consisted of sixteen smaller sample plots (50 m × 50 m), with 537 effective samples including 396, 80 and 61 sample plots of desert, steppe and meadow regions in the basin, respectively. The shooting time of the camera was at approximately 12 o'clock from July to August 2016 to avoid the influence of solar illumination on the image. The shooting height was 30 m.

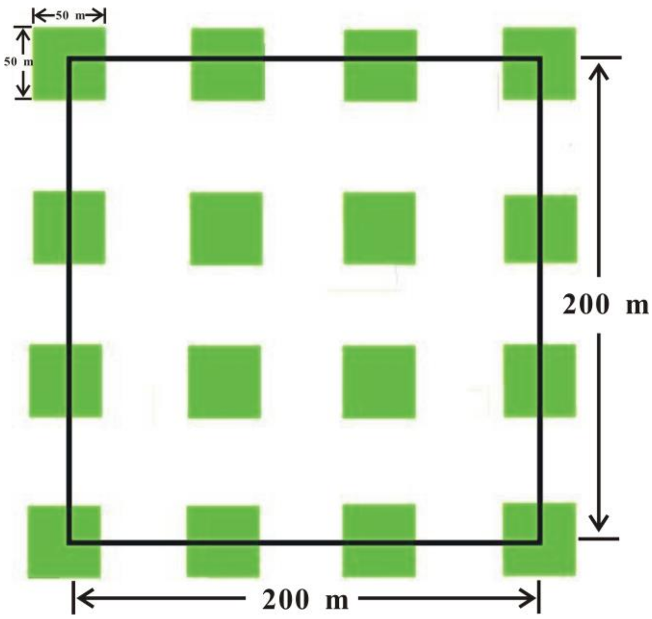

Figure 2. Design of Sample Site (the sample site is 200 m × 200 m, with each sample site including 16 sample plots with 50 m × 50 m; the shooting point of the UAV is at the center of the sample plot).

The data of vegetation types were based on the 1:1 million Chinese vegetation map compiled by the Institute of Botany, Chinese Academy of Sciences (2001). The map is classified by vegetation communities named after the dominant species. In the vegetation map, the communities were divided into 11 vegetation type groups (e.g., desert, steppe, meadow and forest, etc.) and 54 vegetation types (e.g., alpine steppe, temperate steppe, etc.) according to community and habitat characteristics. We adopted vegetation type groups to divide vegetation regions of Qaidam Basin. Because of the inconsistency of resolution between the sample plots (50 m × 50 m) and the remote sensing image (30 m × 30 m), we chose the shooting point from the UAV (image centre position) as the sample point to match the remote sensing data, which might have resulted in a certain deviation of a small number of pixel values. ArcGIS 10.2 was used to overlay the ground sample plots onto a vector diagram of vegetation types, and the map was classified further according to a field sample survey due to the deviation in the precision between the vegetation atlas (2001) and measured data (2016). The vegetation type of each sample plot in the study area was acquired.

Landsat8-OLI (www.gscloud.cn) was selected for the remote sensing data with a total of 25 images. Its average cloud cover was 3.4%. The images were taken from June 16 to September 9 in 2016, with a spatial resolution of 30 m. The remote data acquisition time was almost identical to the ground-measured data, which can best reflect the FVC. To determine the reflectance of each pixel, the remote sensing image was preprocessed with radiometric calibration and atmospheric correction by ENVI 5.1, and the maximum value composite (MVC) was used to reduce the influence of clouds and the solar altitude angle through the band math tool in ENVI 5.1 [44]. The image data were stitched and cut by ERDAS 9.2 to provide basic data for the FVC inversion in the Qaidam Basin.

3.2. Research Methods

3.2.1. Measured Data Processing

There is no significant difference between the FVC and the true coverage value identified by the threshold adjustment method [11]. The basic principle of this method is to set the threshold of the excess greenness index (EGI) and compare it with each pixel to get the vegetation information. When the pixel is larger than this threshold, it is a vegetation pixel; otherwise it is a non-vegetation pixel [45]. We used the threshold adjustment method to distinguish vegetation and non-vegetation information (Figure 3). This method can accurately identify the steppe community and the meadow community. However, the desert community consists of a single or a few desert shrubs. The color of individual species of desert shrubs, such as *Ceratoides latens* in the Qaidam Basin, is close to that of the bare land, which makes vegetation not easy to be identified. Therefore, we performed visual interpretation in Photoshop to replace the unrecognizable vegetation part with similar color and then applied the threshold adjustment method to identify the extracted vegetation information (Figure 3e). A more accurate measurement of FVC was finally obtained.

$$\begin{cases} \text{EGI} = \text{2Green band} - \text{Red band} - \text{Blue band} \\ \text{EGI} > \text{threshold} \quad \text{vegetation pixel} \\ \text{EGI} < \text{threshold} \quad \text{non-vegetation pixel} \end{cases} \tag{1}$$

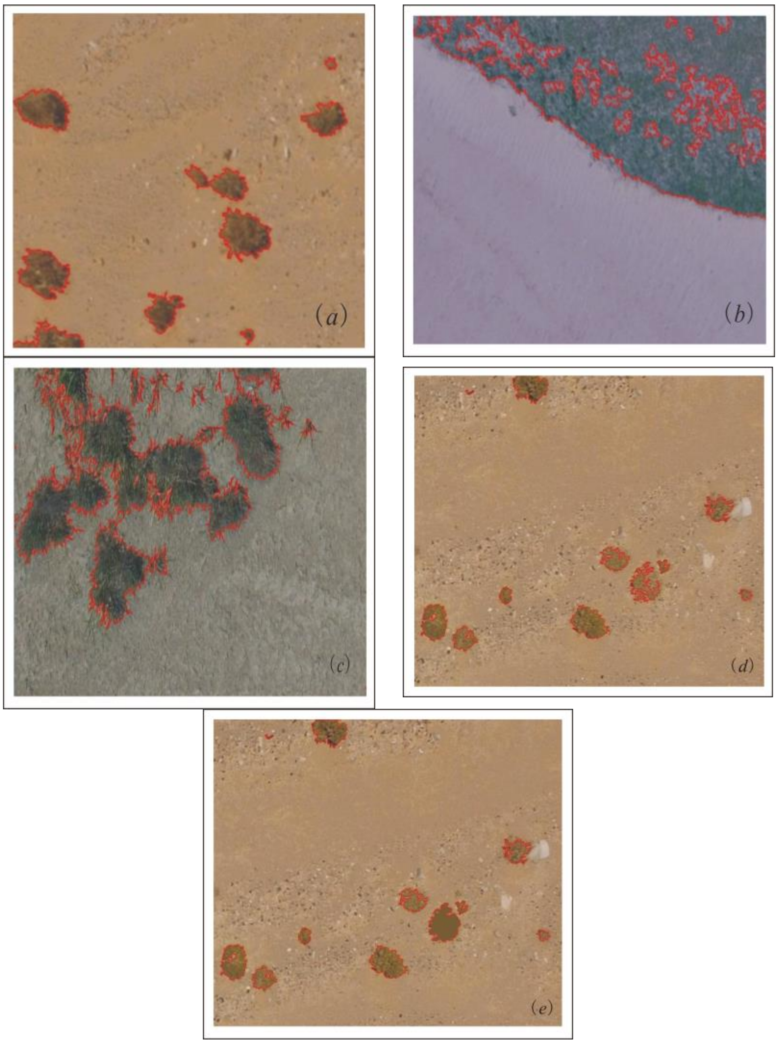

Figure 3. Local identification of FVC by the threshold adjustment method ((**a**): desert; (**b**): steppe; (**c**): meadow; (**d**): desert vegetation recognized by threshold adjustment; (**e**): desert vegetation recognized by threshold adjustment and visual interpretation).

3.2.2. Vegetation Classification Inversion and Vegetation Mixed Inversion of FVC

The condition of the underlying surface is complicated in the Qaidam Basin, which leads to wide variations in FVC values. In order to improve the accuracy of FVC, we tried to divide the vegetation in the basin into different communities to estimate FVC by different models (vegetation classification inversion, VCI) according to the Vegetation Atlas and field survey. The results were compared with FVC determined by vegetation mixed inversion (VMI, including desert, steppe and meadow communities) in the entire study area. The detailed features of FVC estimation using different methods and at different scales are presented below.

3.2.3. Empirical Model

An EM is developed based on a VI value and the actual FVC [21]. The relationships between VIs and FVC are diverse and depend on the different band combinations and operation methods employed [46]. Visible and near-infrared bands are the most sensitive bands to vegetation and can filter out the influence of many factors such as grass background and crown shadow [19]. The normalized difference vegetation index (NDVI), ratio vegetation index (RVI), difference vegetation index (DVI), modified vegetation index (MVI), modified soil-adjusted vegetation index (MSAVI) and normalized difference greenness index (NDGI) were calculated by using the visible and near-infrared wavelengths of Landsat8 (Table 1). We analyzed the correlation between different VIs and the FVC and selected the optimum VI and the measured FVC of desert, steppe and meadow regions of the basin for regression analysis. Basing on the ground-measured data with camera in spots and corresponding VI data from Landsat8, a reasonable empirical model of the FVC estimation was established. Finally, we substituted each pixel of VI into the established regression equation to estimate the FVC of the whole regions.

Table 1. Formulas for calculating different vegetation indexes.

Vegetation Index	Calculation Formula
Normalized Difference Vegetation Index (NDVI)	$NDVI = (NIR - R)/(NIR + R)$
Ratio Vegetation Index (RVI)	$RVI = NIR/R$
Difference Vegetation Index (DVI)	$DVI = NIR - R$
Modified Vegetation Index (MVI)	$MVI = \sqrt{(NIR - R)/(NIR + R) + 0.5}$
Modified Soil-Adjusted Vegetation Index (MSAVI)	$MSAVI = (2NIR + 1 - \sqrt{(2NIR + 1)^2 - (8NIR - R)})/2$
Normalized Difference Greenness Index (NDGI)	$NDGI = (G - R)/(G + R)$

Note: *NIR* is near-infrared band reflectance; *R* is red band reflectance; *G* is green band reflectance.

3.2.4. Pixel Decomposition Model

For the PDM, the spectral information (S) received by the sensor is composed of the vegetation cover (S_{veg}) and non-vegetation cover (S_0) information; the information contributed by S_{veg} can be expressed as the product of the information of pure vegetation (S_v) and the ratio of vegetation cover to pixels (f_c), while the information contributed by S_0 is the product of the pure soil pixels (S_s) and $(1 - f_c)$ [32,47]:

$$S_{veg} = S_v \times f_c \tag{2}$$

$$S_0 = S_s \times (1 - f_c) \tag{3}$$

$$f_c = \frac{S - S_s}{S_v - S_s} \tag{4}$$

The NDVI pixels can reflect the growth conditions and cover changes of vegetation effectively, and it has widely been calculated using Formula (3) to invert FVC [48]:

$$f_c = \frac{NDVI - NDVI_s}{NDVI_v - NDVI_s} \tag{5}$$

where f_c is FVC; $NDVI$ is a weighted average of vegetation and non-vegetation regions; $NDVI_s$ is the vegetation index of the bare soil pixels; and $NDVI_v$ is the vegetation index of the whole vegetation cover.

For most types of bare surfaces, $NDVI_s$ can be affected by many factors such as surface roughness, soil moisture content and weather [10]. The selection of $NDVI_v$ and $NDVI_s$ greatly affects the inversion precision of FVC [49]. According to the field investigation and test of multiple measured data, we selected NDVI values of the inflection point of the cumulative histogram as the $NDVI_s$ values for the

PDM for the desert, steppe, meadow and mixed vegetation regions of the basin and took the maximum value of NDVI as $NDVI_v$. The distribution of FVC by PDM in the Qaidam Basin was obtained by applying the formulas above.

3.2.5. Accuracy Evaluation

The accuracy of the EM and PDM was verified based on measured data. The root mean square error (RMSE), mean absolute error (MAE), average relative error (ARE) and coefficient of determination (R^2) were chose as the evaluation indexes:

$$RMSE = \sqrt{\frac{1}{N}\sum_{i=1}^{N}(T_i - T_i^*)^2} \tag{6}$$

$$MAE = \frac{1}{N}\sum_{i=1}^{N}(|T_i - T_i^*|) \tag{7}$$

$$ARE = \frac{1}{N}\sum_{i=1}^{N}\left|\frac{T_i - T_i^*}{T_i} \times 100\%\right| \tag{8}$$

$$R^2 = \sum_{i=1}^{N}(T_i^* - \overline{T})^2 / \sum_{i=1}^{N}(T_i - \overline{T})^2 \tag{9}$$

where T_i and T_i^* stand for the measured value and predicted value for sample i, respectively; $\overline{T}$ represents the average value of the measured value; and N is the number of samples. $RMSE$ and R^2 are measures of bias. The smaller the $RMSE$ value is, the smaller the estimated deviation; the closer R^2 is to 1, the better the fitting effect of the equation by the model. ARE and MAE are measures of accuracy. The smaller the values of ARE and MAE are, the smaller errors between the predicted value and the measured value and the higher the inversion model accuracy.

4. Results and Analysis

4.1. Inversion of the FVC by the EM

4.1.1. The Construction of the EM

We selected the same number of measured data and corresponding VIs randomly for correlation analysis (Table 2). In general, the VIs were significantly correlated with FVC of different vegetation types ($p < 0.05$), except for NDGI and MSAVI. The FVC of the desert, steppe and meadow regions of the basin had a significant positive correlation with the NDVI ($R > 0.85$) that was much higher than the correlations with other VIs. Therefore, the measured data from 45 randomly selected samples and the corresponding NDVI from different vegetation types were used for regression analysis (Figure 4). The result revealed a nearly linear relationship between the FVC and NDVI ($R^2 > 0.7$, $p < 0.01$). The R^2 in the EM for mixed vegetation region was lower than that for the desert and meadow regions but slightly higher than that for the steppe region.

Table 2. Correlation between vegetation index and fractional vegetation cover.

	NDVI	**RVI**	**DVI**	**MSAVI**	**MVI**	**NDGI**
FVC of desert	0.922 **	−0.762 **	0.769 **	0.220	0.756 **	−0.303 *
FVC of steppe	0.853 **	−0.627 **	0.740 **	0.686 **	0.643 **	0.432 **
FVC of meadow	0.907 **	−0.740 **	0.852 **	0.808 **	0.812 **	0.697 **
FVC of mixed vegetation	0.856 **	−0.739 **	0.679 **	0.649 **	0.864 **	0.161

Note: ** Significantly correlated at the 0.01 level; * significantly correlated at the 0.05 level.

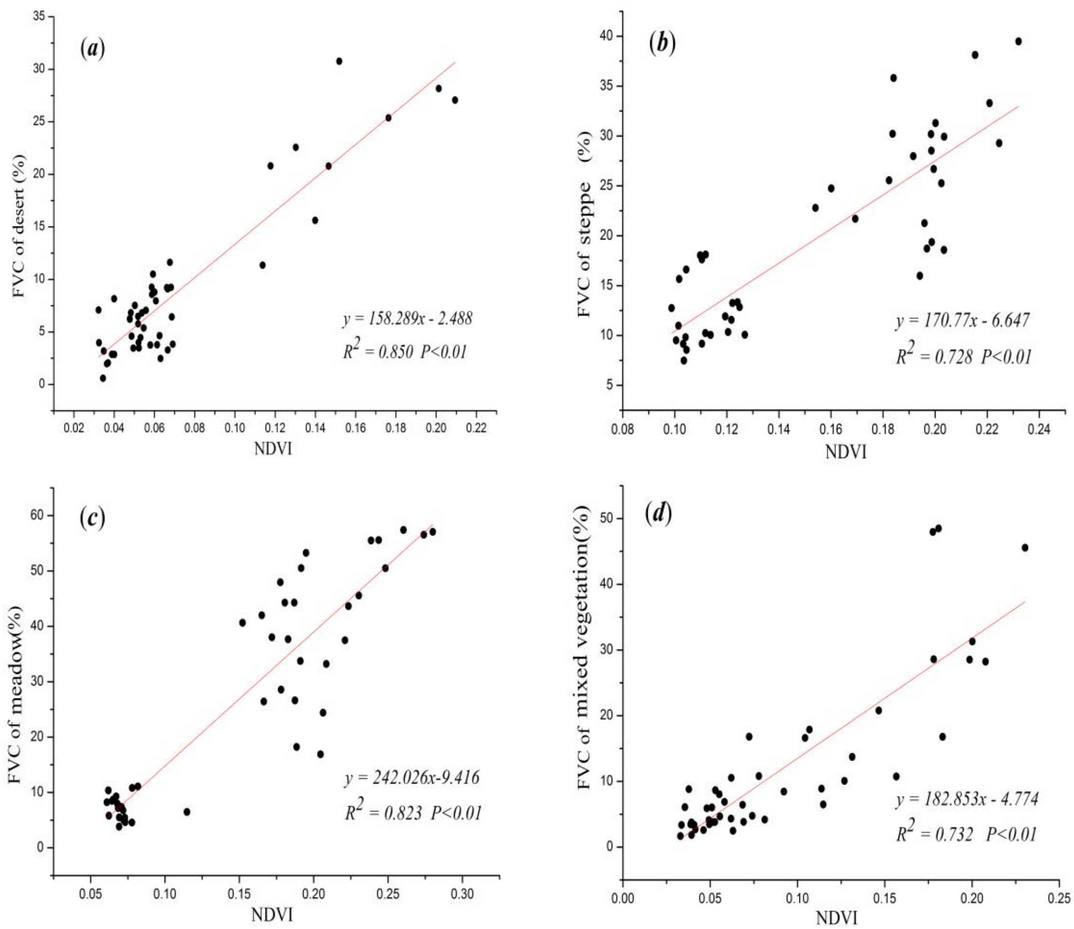

Figure 4. Regression model between the NDVI and FVC ((**a**): desert; (**b**): steppe; (**c**): meadow; (**d**): mixed vegetation).

4.1.2. Inversion of the FVC by the EM

The distribution of the FVC of the desert, steppe, meadow and mixed vegetation regions in the Qaidam Basin were obtained with EM (Figure 5). The distribution trends of the FVC by VCI and VMI were similar and demonstrated a semi-ring pattern decreasing inland from the east and the southeast to the northwest. However, there were significant spatial differences in the FVC at different scales in the basin, primarily in meadow region of the basin with relatively high-density vegetation cover (FVC > 60%). This difference mainly manifests in the *Kobresia willd* communities in the eastern part of the low mountain and intermountain region of the basin, the southwest Kunlun Mountains, the *Phragmite australis—Nitraria tangutorum—Tamarix chinensis* communities in the core area of the oasis in the leading edge of the Golmud-Numhon borderline in the central basin and the *Kobresia humilis* communities in the southern piedmont area of the Qilian Mountains. In addition, there was a significant difference in the *Stipa purpurea* communities in the southern Kunlun Mountains. The FVC were similar in the desert region and the northwest steppe region with extremely low-density vegetation cover (FVC $\leq$ 10%), which is mainly in the piedmont plain of the northern slope of the Kunlun Mountains in the southwestern basin, Altun Mountain in the northwest intermountain basin, and the flat terrain in the middle basin. The average FVC values according to the VCI and VMI of the *Ceratoides latens—Sympegma regelii* communities and *Stipa purpurea* communities were 11.49% and 11.38%, respectively.

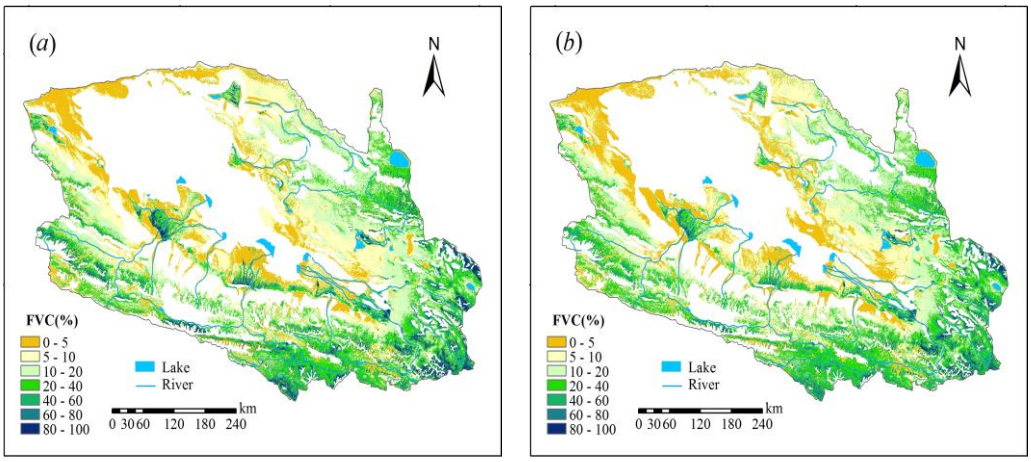

Figure 5. Inversion of FVC by the EM. (**a**): VCI by EM; (**b**): VMI by EM.

4.2. Inversion of the FVC by the PDM

The VCI and VMI estimated by the PDM also showed a semi-ring decreasing trend from the east and southeast to the northwest of the basin (Figure 6), and the average FVC was 16.5% and 13.8% respectively. VCI produced lower inversion values in extremely low-density vegetation cover areas and higher inversion values in high-density vegetation cover areas (FVC > 80%). Differences in FVC were mainly in the central and western regions of the basin, the low mountains and intermountain basin to the east of Dulan, and the southwest Kunlun Mountains. The area of extremely low-density vegetation cover accounted for 52% of the total area in Figure 6a, of which FVC $\leq$ 5% accounted for 22.5%. However, the extremely low-density vegetation cover regions are located in the central part of the basin in Figure 6b, primarily in the southwest Da Qaidam-Delingha borderline and the surrounding Gasikule Lake, and the area of FVC $\leq$ 5% only accounted for 13%. Similarly, meadow region of the basin, which are mainly distributed in the low mountains and intermountain basin to the east of Dulan, the mountainous steppe region to the south of Xiangride and regions at the front edge of the alluvial-proluvial fan such as the narrow strip of oasis to the north of the Golmud-Numhon borderline, also exhibited the most obvious differences in FVC.

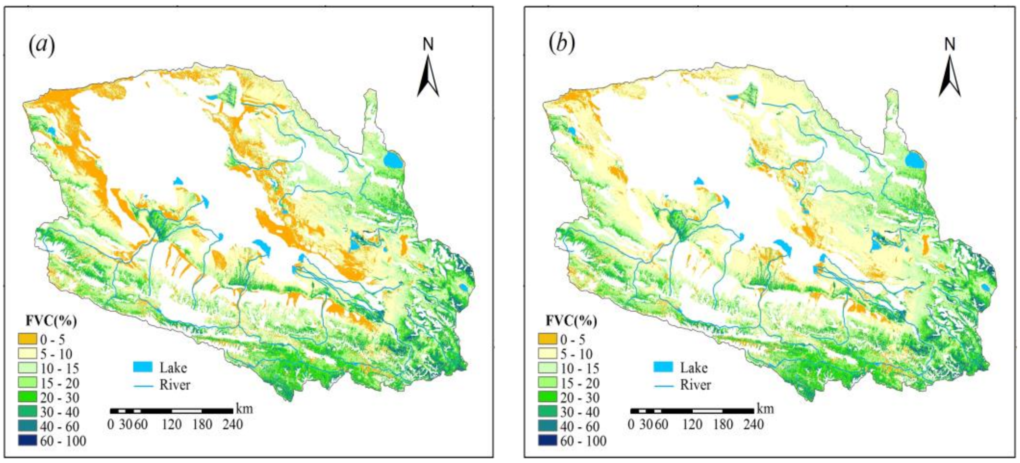

Figure 6. Inversion of FVC by the PDM. (**a**): VCI by PDM; (**b**): VMI by PDM.

4.3. Comparison of VCI Estimated by the EM and PDM

The same estimation method yielded different results at different spatial scales, and the inversion results of the same vegetation types by different methods exhibited significant differences. The desert region where the FVC was concentrated below 15% according to the PDM accounted for 90%, with an average coverage 3.4% lower than that estimated by the EM. The vegetation types of the extremely low-density and low-density vegetation cover areas (10% < FVC ≤ 20%) were *Ceratoides latens* communities in the western and northern parts of the basin and the eastern *Haloxylon ammodendron* communities, the *Nitraria tangutorum* communities and the *Salsola collina* communities in the southwest valley. The average FVC was 12.2% according to the EM. The area of lower-density vegetation cover (20% < FVC ≤ 40%) was mainly distributed in the front of the alluvial-proluvial fan in the southern Golmud-Nomhon borderline of the basin center, and the vegetation in this area is dominated by *Tamarix chinensis* and *Artemisia desertorum*, with a smaller contribution from *Ceratoides latens*, *Calligonum mongolicum* and *Sympegma regelii*. Only 5% of the area has lower-density vegetation cover, as shown in Figure 7b, which is distributed sporadically in the *Artemisia desertorum* communities of eastern Dulan.

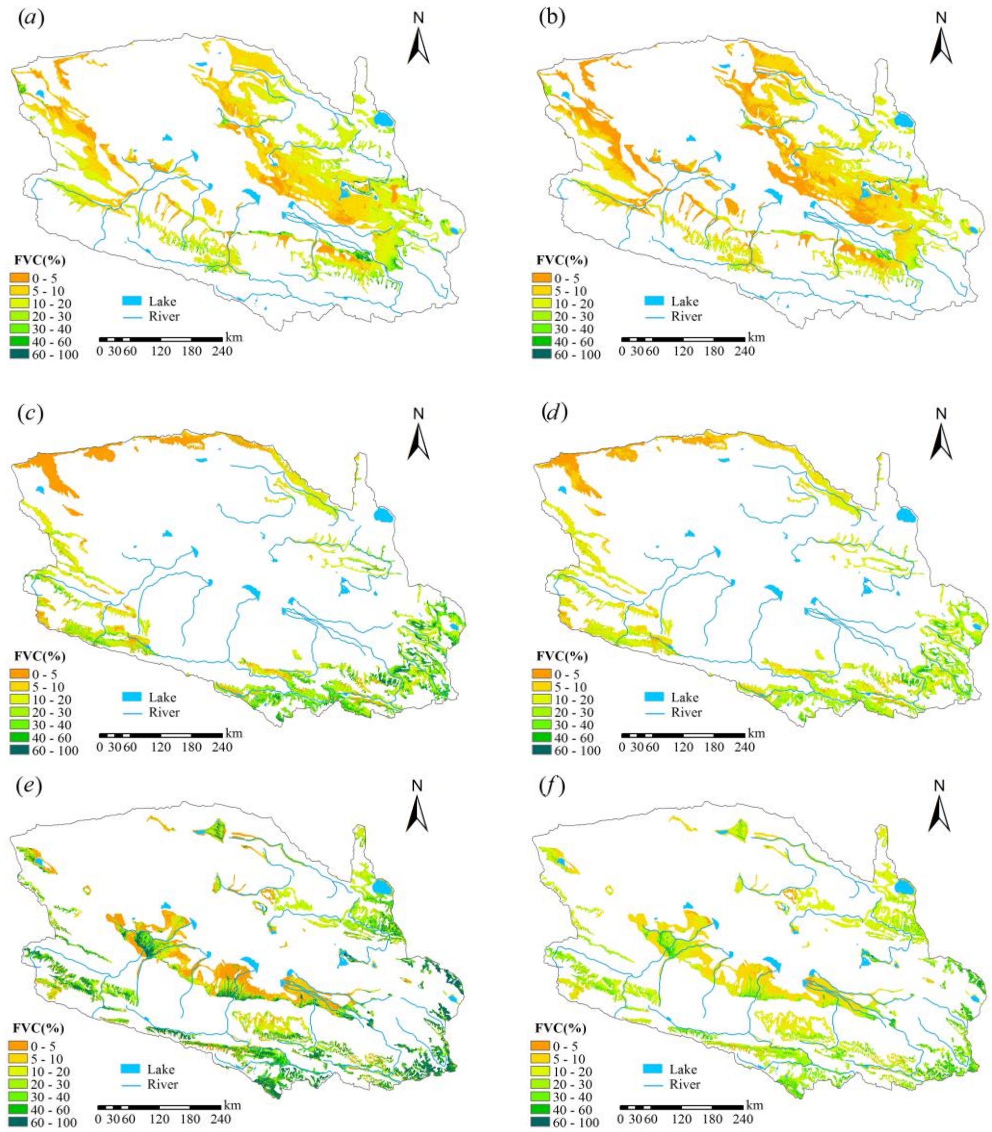

Figure 7. VCI of fractional vegetation cover by the EM and PDM ((**a**): desert FVC by EM inversion; (**b**): desert FVC by PDM inversion; (**c**): steppe FVC by EM inversion; (**d**): steppe FVC by PDM inversion; (**e**): meadow FVC by EM inversion; (**f**): meadow FVC by PDM inversion).

The differences between the FVC estimation of steppe region of the basin by the EM and PDM are reflected in the area of medium-high-density vegetation cover (60% < FVC ≤ 80%) such as the southeastern low mountains and the intermountain basin, for which the dominant vegetation species are *Achnatherum splendens* and *Stipa purpurea*. The FVC retrieved by the PDM was slightly lower than that of the EM. The FVC in the central and western *Stipa purpurea* communities were approximately 5–15%, while the FVC was up to 15% in the eastern regions.

The FVC estimation of meadow by the PDM was lower than that of the EM, and the difference in average coverage was 5%, mainly distributed in high-density vegetation coverage regions such as the *Kobresia tibetica* and *Kobresia humilis* communities in the southeast mountain and valley and *Phragmites australis—Nitraria tangutorum—Tamarix chinensis* communities in the core of the oasis of the Golmud-Nomhon borderline in the basin center. The area of FVC > 60% according to the PDM accounted for 9.8%, while the value was approximately 16.3% according to the EM. The inversion results were similar in the central and northern areas of the basin, with the FVC value mostly ranging from 5% to 15%, with *Phragmites australis*, *Nitraria tangutorum* and *Stebbinsia umbrella* as the predominant vegetation components.

4.4. Ground Verification and Accuracy Evaluation

The VMI according to the EM was more discrete than the VCI. The VCI estimated by the EM provided an ideal effect on FVC inversion with different densities, especially for the area of FVC > 20%. In contrast, an overestimation occurred in low-density vegetation cover steppe region of the basin for the VMI estimated by the EM, and in the area of FVC > 30%, the frequency of abnormal values was higher (Figure 8b).

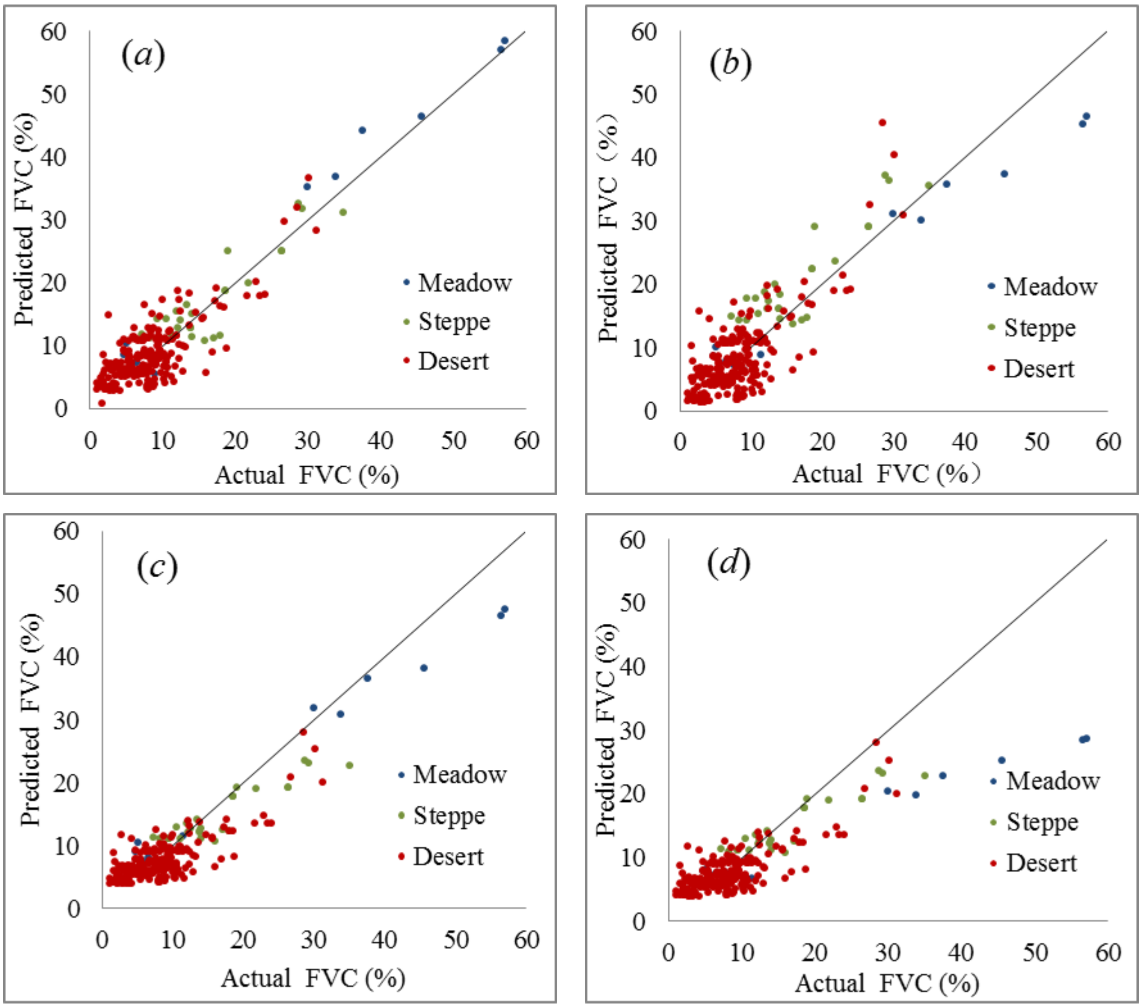

Figure 8. Relationship between actual and predicted FVC ((**a**): VCI accuracy by EM; (**b**): VMI accuracy by EM; (**c**): VCI accuracy by PDM; (**d**): VMI accuracy by PDM).

The difference in FVC estimated by the PDM at different scales was significant. In most instances, VCI performed obviously better than VMI in the meadow region of the basin (Table 3). In addition, FVC was relatively well estimated by the PDM for the desert region and steppe region covered by extremely low-density vegetation cover. However, this method produced an underestimation in the area of FVC > 10%, especially a substantial underestimation by VMI when FVC exceeded 15%, and this underestimation was particularly evident in meadow region estimated by VMI.

Table 3. Inversion accuracy of FVC for different methods and different scales.

	VCI by EM			VMI by EM			VCI by PDM			VMI by PDM		
	D	**G**	**M**	**D**	**G**	**M**	**D**	**G**	**M**	**D**	**G**	**M**
MAE	2.59	2.81	2.91	3.00	3.81	3.34	2.76	3.32	4.35	2.61	3.05	5.96
ARE	0.42	0.30	0.39	0.45	0.39	0.39	0.36	0.27	0.31	0.43	0.27	0.39
RMSE	3.29	3.15	3.77	3.94	4.41	4.35	3.74	4.38	4.93	3.43	3.97	9.39
R^2	0.619	0.788	0.960	0.597	0.788	0.953	0.616	0.813	0.976	0.598	0.825	0.946

Note: D is desert; G is steppe; M is meadow.

For the inversion of FVC by different methods at the same scale, the EM and PDM more accurately estimated the FVC in desert region with extremely low-density vegetation cover (Figure 8). Generally, the error between most predicted values and measured values was approximately 2% and the frequency of abnormal values was the lowest. With the increase of FVC, the values predicted by VMI with PDM inversion were significantly underestimated in the steppe and meadow regions, while the VCI by PDM fit better with higher inversion accuracy (Table 3). The VCI with the EM provided the most ideal results.

5. Discussion and Conclusions

5.1. Discussion

The EM has been proved to be a simple and efficient method for estimating FVC [50]. Purevdorj [51] indicated that the EM has a better accuracy in FVC estimation when a large amount of measured date are available. In this study, we estimated the FVC based on the VMI with 537 sample plots in a complex area. The result showed that the VMI estimated by the EM was ideal, especially for extremely low-density vegetation cover, which was consistent with previous conclusions [22,25]. However, we also found an overestimation of FVC by VMI in most steppe regions with medium-low-density vegetation cover (20% < FVC $\leq$ 40%), and in previous results, the fitting accuracy of this approach was shown to be lower than that for desert and meadow regions (Figure 4). The inland area, located in the northwestern part of the basin, has an arid climate and scarce precipitation, and the southeast and southwest mountainous areas have more windward slope precipitation with higher elevations and snowmelt volume. The hydrological conditions in the southeast and southwest provide more abundant moisture than those in the northwest. The complicated spatial heterogeneity in the Qaidam Basin causes the considerable differences in the FVC between the alpine steppe and temperate steppe regions. In addition, the FVC value of steppe region is mostly between those of desert and meadow regions. When the vegetation is mixed, the difference between steppe and the other vegetation regions will be expanded, which further exacerbates the inversion error of the steppe region of the basin. Therefore, the accuracy of the traditional EM (VMI) still has some limitations even with sufficient measured data. However, VCI with the EM is an effective solution to this problem.

The PDM is widely used on a large spatial scale because remote sensing data can be acquired in multiple periods and the model establishment is independent of measured data [52]. However, the VMI with the PDM showed unsatisfactory results in the areas where FVC > 15% in this study, which mainly manifested in the continued underestimation of FVC. Delamater [27] concluded that FVC tends to be overestimated in tropical rainforest regions with medium-low-density vegetation cover. Li [35] indicated that FVC was underestimated in medium-density vegetation cover. The different viewpoints are mainly due to the selection of model thresholds such as $NDVI_{soil}$ in different regions [53]. It remains unclear how to extract a more accurate threshold, especially for complex areas such as the Qaidam Basin. Fortunately, a higher precision than that achieved with VMI with PDM can be achieved when the FVC is inverted according to different vegetation types. This finding is similar to the conclusion that the PDM has higher precision in desert regions [18]. Compared with the lower $NDVI_{soil}$ value, VCI limits the FVC information of plants to within a certain threshold, which magnifies the difference between the bare soil pixels, vegetation pixels and pure vegetation pixels to some extent. The extraction of variable endmembers such as inflection points are representative, with the improvement of the accuracy of FVC estimation. VCI can effectively extract the endmembers of PDM to improve FVC accuracy. However, the FVC is slightly underestimated by PDM in the areas where FVC > 15%. The NDVI can not only reflect vegetation cover information but also reveals information on soil moisture and LAI [54]. The FVC values in the central saline-alkali meadow region and some of the southeastern low mountain steppe and meadow regions of the basin are higher than 80%. The increase in FVC causes the NDVI to reach saturation eventually [55]. In addition, the PDM does not rely on the support of measured data. These factors all affect the accuracy of its the inversion effect. Determining how to comprehensively use different parameters to improve the accuracy of model estimation in large-scale studies remains to be further explored.

The comparison of inversion accuracy between EM and PDM has been studied to a certain extent [29,56]. Jiapaer [18] noted that the EM could produce good results for a specified area, but it did not provide ideal accuracy compared with PDM on a large scale due to the influence of the growing season and vegetation types. Xiao [33] showed the predicted and actual values of PDM had a better fitting than those of the EM. However, the issue of how to overcome the limitation of the model has been ignored. In our study, we found that the accuracy of the EM is better than that of the PDM without considering the type of vegetation. In particular, when we tried to invert the FVC according to different vegetation types, the VCI with the EM and PDM produced smaller errors and deviations, especially for the EM. Furthermore, the VCI with the PDM was slightly better than the VMI with the EM. This difference might be attributable to the fact that the method employing VCI transforms a complex environment on a large scale into several single environments at the regional scale, which reduces the spatial variability of complicated regions to some extent and takes into account the variation in different vegetation structures. As a result, the VCI expands the scope of application of the traditional EM under the premise of ensuring local precision and improves the accuracy of FVC inversion of PDM on a wide scale by classifying and simplifying the complexity of the pixels. These advantages may provide promising guidance for future research on FVC estimation.

The accurate acquisition and discernment of ground data is a very complicated and difficult task; therefore, high-resolution remote sensing images are frequently used instead of measured data for model establishment and ground verification [33]. Dymond [12] randomly selected 20 plots based on SPOT images to identify the accuracy of steppe FVC. However, the VI is too coarse for direct verification of the FVC, which will further increase the inversion error of the model [57]. To obtain actual FVC, Li [58] estimated the FVC of steppe regions in northern China and found that the use of the digital camera method yielded the most accurate estimation results, which could be used as the true FVC values. However, the acquisition of ground-based measured data using a digital camera is time consuming and labor intensive [45]. On this basis, taking into account the special terrain and vegetation characteristics in the Qaidam Basin, we used a digital camera with an UAV platform to combine the threshold adjustment method and visual interpretation using Photoshop to identify FVC information multiple times. Efforts were made to eliminate the effects of gravel and soil background, and more accurate measured data were obtained. The application of UAV not only greatly reduced the necessary workload but also reduced restrictions related to regional accessibility and terrain, providing the measured data with a universal relevance in large-scale expansion from the point to surface space.

The continuous development of UAV and digital camera technology has made it possible to acquire ground-measured data extensively and combine these data with remote sensing images to estimate the FVC, representing a useful and sustainable tool for the study of FVC.

In the construction of the inversion model of FVC, uncertainties may also have affected the accuracy of the estimation results. First, we did not consider the effect of LAI under different vegetation types when constructing the model. Second, there was an inconsistency in the resolution of the actual sample (50 m $\times$ 50 m) and Landsat8 data (30 m $\times$ 30 m). Finally, this study did not combine land use data from the same period in the analysis process. Sporadic snow-covered areas in some mountainous regions and construction land such as saltworks and highways were not completely eliminated in the vegetation classification, which caused the model to have a few outliers during the inversion process, and the results were affected to a certain degree.

5.2. Conclusions

The correlation between the NDVI and FVC was the most significant, and the linear regression was ideal ($R^2 > 0.7$) for the desert, steppe and meadow regions in the Qaidam Basin, indicating that NDVI is more suitable for constructing an EM for FVC estimation.

Differences were observed in the FVC estimation between VCI and VMI by the EM in the areas with relatively high-density vegetation cover, and differences in the FVC of PDM occurred in the areas with extremely low-density vegetation cover and high-density vegetation cover. However, the PDM substantially underestimated the FVC in the areas with FVC > 15%, especially with the VMI.

VCI is a promising method to improve the accuracy of FVC estimation on a large scale, providing higher precision for both the EM and the PDM. The performance of VCI with the EM provided the best result, and VMI with the PDM provided the worst result.

The VCI of the EM showed the highest simulation accuracies. The FVC of desert, steppe and meadow regions in the Qaidam Basin generally reflected a semi-ring decreasing trend from the east and southeast to the northwest. Approximately 40% of the area with extremely low-density vegetation cover was located in the *Ceratoides latens* communities in the mid-western part and the *Stipa purpurea* communities at the northwestern margin of the basin, and the area with FVC $\leq$ 5% accounted for 21.5%. The areas with lower-density vegetation cover were mainly located in the southwest Kunlun Mountains and the southeastern valley of the basin, which are mainly vegetated by *Stipa purpurea* and *Kobresia species*. The areas with middle-density and high-density vegetation cover were mainly distributed in the front of the alluvial-proluvial fan of the northern oasis of the Golmud-Nomhon borderline of the eastern low mountains. These steppe and meadow regions mainly comprised species of *Achnatherum splendens*, *Stipa purpurea* and *Artemisia desertorum*.

Author Contributions: Writing—Original Draft Preparation, S.Z.; Project Administration, H.C.; Software, Y.F.; Validation, H.N.; Investigation, Y.Y. and B.Z.

Funding: This research was funded by the National Natural Science Foundation of China (grant number: 40971118).

Conflicts of Interest: The authors declare no conflict of interest.

References

1. Yao, J.; He, X.Y.; Li, X.Y.; Chen, W.; Tao, D.L. Monitoring responses of forest to climate variations by MODIS NDVI: A case study of Hun River upstream, northeastern China. *Eur. J. For. Res.* **2012**, *131*, 705–716. [CrossRef]
2. Chen, X.Q.; Wang, H. Spatial and temporal variations of vegetation belts and vegetation cover degrees in Inner Mongolia from 1982 to 2003. *Acta Geogr. Sin.* **2009**, *64*, 84–94.
3. Gitelson, A.A.; Kaufman, Y.J.; Stark, R.; Rundquist, D. Novel algorithms for remote estimation of vegetation fraction. *Remote Sens. Environ.* **2002**, *80*, 76–87. [CrossRef]

4. Gao, Y.N.; Gao, J.F.; Wang, J.; Wang, S.S.; Li, Q.; Zhai, S.H.; Zhou, Y. Estimating the biomass of unevenly distributed aquatic vegetation in a lake using the normalized water-adjusted vegetation index and scale transformation method. *Sci. Total Environ.* **2017**, *601*, 998–1007. [CrossRef] [PubMed]
5. Wen, J.; Lai, X.; Pan, X.D.; Pan, X.D. Numerical simulations of fractional vegetation coverage influences on the convective environment over the source region of the Yellow River. *Meteorol. Atmos. Phys.* **2013**, *120*, 1–10. [CrossRef]
6. Zhou, Z.C.; Shangguan, Z.P.; Zhao, D. Modeling vegetation coverage and soil erosion in the loess plateau area of China. *Ecol. Model.* **2006**, *198*, 263–268. [CrossRef]
7. Yan, Y.; Xu, X.; Xin, X.; Yang, G.X.; Wang, X.; Yan, R.R.; Chen, B.R. Effect of vegetation coverage on Aeolian dust accumulation in a semiarid steppe of northern China. *Catena* **2011**, *87*, 351–356. [CrossRef]
8. Yuan, L.; Zhang, L.Q. Mapping large-scale distribution of submerged aquatic vegetation coverage using remote sensing. *Ecol. Inform.* **2008**, *3*, 245–251. [CrossRef]
9. Gu, X.P.; Huang, M.; Ji, J.J.; Wu, Z.P. The influence of climate change on vegetation net primary productivity in southwestern china during recent 20 years period. *J. Nat. Resour.* **2007**, *22*, 251–259.
10. Qi, J.; Marsett, R.C.; Moran, M.S.; Goodrich, D.; Heilman, P.; Kerr, Y.H.; Dedieu, G.; Chehbouni, A.; Zhang, X.X. Spatial and temporal dynamics of vegetation in the san Pedro river basin area. *Agric. For. Meteorol.* **2000**, *105*, 55–68. [CrossRef]
11. Yi, S.H.; Zhou, Z.Y.; Ren, S.L.; Xu, M.; Qin, Y.; Chen, S.Y.; Ye, B.S. Effects of permafrost degradation on alpine grassland in a semi-arid basin on the Qinghai-Tibetan plateau. *Environ. Res. Lett.* **2011**, *6*, 45403–45409. [CrossRef]
12. Dymond, J.R.; Stephens, P.R.; Newsome, P.F.; Wilde, R.H. Percentage vegetation cover of a degrading rangeland from SPOT. *Int. J. Remote Sens.* **1992**, *13*, 1999–2007. [CrossRef]
13. Liu, X.; Zhou, W.; Bai, Z. Vegetation coverage change and stability in large open-pit coal mine dumps in china during 1990–2015. *Ecol. Eng.* **2016**, *95*, 447–451. [CrossRef]
14. Atzberger, C.; Rembold, F. Mapping the spatial distribution of winter crops at sub-pixel level using AVHRR NDVI time series and neural nets. *Remote Sens.* **2013**, *5*, 1335–1354. [CrossRef]
15. Hansen, M.C.; Defries, R.S.; Townshend, J.R.G.; Sohlberg, R.A.; Dimiceli, C.; Carroll, M.L. Towards an operational MODIS continuous field of percent tree cover algorithm: Examples using AVHRR and MODIS data. *Remote Sens. Environ.* **2002**, *83*, 303–319. [CrossRef]
16. Tottrup, C.; Rasmussen, M.S.; Eklundh, L.; Jönsson, P. Mapping fractional forest cover across the highlands of mainland southeast Asia using MODIS data and regression tree modelling. *Int. J. Remote Sens.* **2007**, *28*, 23–46. [CrossRef]
17. Scarth, P.; Phinn, S. Determining forest structural attributes using an inverted geometric-optical model in mixed eucalypt forests, southeast Queensland, Australia. *Remote Sens. Environ.* **2000**, *71*, 141–157. [CrossRef]
18. Jiapaer, G.; Chen, X.; Bao, A. A comparison of methods for estimating fractional vegetation cover in arid regions. *Agric. For. Meteorol.* **2011**, *151*, 1698–1710. [CrossRef]
19. Chen, Y.H.; Shi, P.J.; Li, X.B.; Chen, J. A combined approach for estimating vegetation cover in urban/suburban environments from remotely sensed data. *Comput. Geosci.* **2006**, *32*, 1299–1309.
20. Peter, R.J. North estimation of fAPRA, LAI, and vegetation fractional cover from ATSR-2 imagery. *Remote Sens. Environ.* **2002**, *80*, 114–121.
21. Gu, Z.J.; Ju, W.M.; Li, L.; Li, D.P.; Liu, Y.B.; Fan, W.L. Using vegetation indices and texture measures to estimate vegetation fractional coverage (VFC) of planted and natural forests in Nanjing city, China. *Adv. Space Res.* **2013**, *51*, 1186–1194. [CrossRef]
22. Jakubauskas, M.; Kindscher, K.; Fraser, A.; Debinski, D.M.; Price, K. Close-range remote sensing of aquatic macrophyte vegetation cover. *Int. J. Remote Sens.* **2000**, *21*, 3533–3538. [CrossRef]
23. Voorde, T.D.V.; Vlaeminck, J.; Canters, F. Comparing different approaches for mapping urban vegetation cover from Landsat ETM+ data: A case study on Brussels. *Sensors* **2008**, *8*, 3880–3902. [CrossRef] [PubMed]
24. Boyd, D.S.; Foody, G.M.; Ripple, W.J. Evaluation of approaches for forest cover estimation in the Pacific Northwest, USA, using remote sensing. *Appl. Geogr.* **2002**, *22*, 375–392. [CrossRef]
25. Purevdorj, T.S.; Tateishi, R.; Ishiyama, T. Relationships between percent vegetation cover and vegetation indices. *Int. J. Remote Sens.* **1998**, *19*, 3519–3535. [CrossRef]

26. Delamater, P.L.; Messina, J.P.; Qi, J.; Cochrane, M.A. A hybrid visual estimation method for the collection of ground truth fractional coverage data in a humid tropical environment. *Int. J. Appl. Earth Obs. Geoinf.* **2012**, *18*, 504–514. [CrossRef]
27. Zhang, X.F.; Liao, C.H.; Li, J.; Sun, Q. Fractional vegetation cover estimation in arid and semi-arid; environments using hj-1 satellite hyperspectral data. *Int. J. Appl. Earth Obs. Geoinf.* **2013**, *21*, 506–512. [CrossRef]
28. Lehnert, L.W.; Meyer, H.; Wang, Y.; Miehe, G.; Thies, B.; Reudenbach, C.; Bendix, C. Retrieval of grassland plant coverage on the Tibetan Plateau based on a multi-scale, multi-sensor and multi-method approach. *Remote Sens. Environ.* **2015**, *164*, 197–207. [CrossRef]
29. Asner, G.P.; Heidebrecht, K.B. Spectral unmixing of vegetation, soil and dry carbon cover in arid regions: Comparing multispectral and hyperspectral observations. *Int. J. Remote Sens.* **2002**, *23*, 3939–3958. [CrossRef]
30. Donohue, R.J.; Mcvicar, T.R.; Roderick, M.L. Climate-related trends in Australian vegetation cover as inferred from satellite observations, 1981–2006. *Glob. Chang. Biol.* **2010**, *15*, 1025–1039. [CrossRef]
31. Omuto, C.T.; Vargas, R.R.; Alim, M.S.; Paron, P. Mixed-effects modelling of time series NDVI-rainfall relationship for detecting human-induced loss of vegetation cover in drylands. *J. Arid Environ.* **2010**, *74*, 1552–1563. [CrossRef]
32. Gutman, G.; Ignatov, A. The derivation of the green vegetation fraction from NOAA/AVHRR data for use in numerical weather prediction models. *Int. J. Remote Sens.* **1998**, *19*, 1533–1543. [CrossRef]
33. Xiao, J.; Moody, A. A comparison of methods for estimating fractional green vegetation cover within a desert-to-upland transition zone in central New Mexico, USA. *Remote Sens. Environ.* **2005**, *98*, 237–250. [CrossRef]
34. Filipponi, F.; Valentini, E.; Xuan, A.N.; Guerra, G.A.; Wolf, F.; Andrzejak, M.; Taramelli, A. Global MODIS Fraction of Green Vegetation Cover for Monitoring Abrupt and Gradual Vegetation Changes. *Remote Sens.* **2018**, *10*, 653. [CrossRef]
35. Li, F.; Chen, W.; Zeng, Y.; Zhao, Q.J.; Wu, B.F. Improving estimates of grassland fractional vegetation cover based on a pixel dichotomy model: A case study in Inner Mongolia, China. *Remote Sens.* **2014**, *6*, 4705–4722. [CrossRef]
36. Peterson, S.H.; Stow, D.A. Using multiple image endmember spectral mixture analysis to study chaparral regrowth in southern California. *Int. J. Remote Sens.* **2003**, *24*, 4481–4504. [CrossRef]
37. Shoshany, M.; Svoray, T. Multidate adaptive unmixing and its application to analysis of ecosystem transitions along a climatic gradient. *Remote Sens. Environ.* **2002**, *82*, 5–20. [CrossRef]
38. Jiang, Z.Y.; Huete, A.R.; Chen, J.; Chen, Y.H.; Li, J.; Yan, G.J.; Zou, Y. Analysis of NDVI and scaled difference vegetation index retrievals of vegetation fraction. *Remote Sens. Environ.* **2006**, *101*, 366–378. [CrossRef]
39. Small, C. High spatial resolution spectral mixture analysis of urban reflectance. *Remote Sens. Environ.* **2003**, *88*, 170–186. [CrossRef]
40. Zhao, Y.; Yu, Z.H.; Chen, F.H.; Ito, E.; Zhao, C. Holocene vegetation and climate history at Hurleg Lake in the Qaidam Basin, northwest China. *Rev. Palaeobot. Palynol.* **2007**, *145*, 275–288. [CrossRef]
41. Xu, X.K.; Chen, H.; Levy, J.K. Spatiotemporal vegetation cover variations in the Qinghai-Tibet Plateau under global climate change. *Chin. Sci. Bull.* **2008**, *53*, 915–922. [CrossRef]
42. Fu, Y.; Chen, H.; Niu, H.H.; Zhang, S.Q.; Yang, Y. Spatial and temporal variation of vegetation phenology and its response to climate changes in Qaidam basin from 2000 to 2015. *J. Geogr. Sci.* **2018**, *28*, 400–414. [CrossRef]
43. Udvardy, M.D.F. *A Classification of the Biogeographical Provinces of the World*; International Union for Conservation of Nature and Natural Resources: Morges, Switzerland, 1975; Volume 8.
44. Brent, N.H. Characteristics of maximum-value composite images from temporal AHVRR data. *Int. J. Remote Sens.* **1986**, *7*, 1417–1434.
45. Chen, J.J.; Yi, S.H.; Yu, Q.; Wang, X.Y. Improving estimates of fractional vegetation cover based on UAV in alpine grassland on the Qinghai–Tibetan plateau. *Int. J. Remote Sens.* **2016**, *37*, 1922–1936. [CrossRef]
46. Catherine, L.; Michel, M.V.; Bernard, P. Evaluation of the performance of various vegetation indices to retrieve vegetation cover from AVHRR data. *Remote Sens. Rev.* **1995**, *10*, 265–284.
47. Zhu, H.L.; Yang, G.H.; Han, L. Analysis of fractional vegetation coverage changes and its influence factors during farmland returned to forest period in Yan'an city. *Trans. Chin. Soc. Agric. Mach.* **2015**, *46*, 272–280.

48. Jing, X.; Yao, W.Q.; Wang, J.H.; Song, X.Y. A study on the relationship between dynamic change of vegetation coverage and precipitation in Beijing's mountainous areas during the last 20 years. *Math. Comput. Model.* **2011**, *54*, 1079–1085. [CrossRef]
49. Wu, C.; Murray, A.T. Estimating impervious surface distribution by spectral mixture analysis. *Remote Sens. Environ.* **2003**, *84*, 493–505. [CrossRef]
50. Patel, N.K.; Saxena, R.K.; Shiwalkar, A. Study of fractional vegetation cover using high spectral resolution data. *J. Indian Soc. Remote Sens.* **2007**, *35*, 73–79. [CrossRef]
51. Purevdorj, T.S.; Ishiyama, T.; Tateishi, R. Estimating of percent vegetation cover using vegetation indices. In Proceedings of the Japan Society for Photogrammetry and Remote Sensing Conference, Yamagata, Japan, 8–9 October 1996; pp. 101–104.
52. Colombo, R.; Bellingeri, D.; Fasolini, D.; Marino, C.M. Retrieval of leaf area index in different vegetation types using high resolution satellite data. *Remote Sens. Environ.* **2003**, *86*, 120–131. [CrossRef]
53. Montandon, L.M.; Small, E.E. The impact of soil reflectance on the quantification of the green vegetation fraction from NDVI. *Remote Sens. Environ.* **2008**, *112*, 1835–1845. [CrossRef]
54. Li, Z.; Zhang, Y.; Zhu, Q.; He, Y.M.; Yao, W.J. Assessment of bank gully development and vegetation coverage on the Chinese loess plateau. *Geomorphology.* **2015**, *228*, 462–469. [CrossRef]
55. Carlson, T.N.; Perry, E.M.; Schmugge, T.J. Remote estimation of soil moisture availability and fractional vegetation cover for agricultural fields. *Agric. For. Meteorol.* **1990**, *52*, 45–69. [CrossRef]
56. Buyantuyev, A.; Wu, J.; Gries, C. Estimating vegetation cover in an urban environment based on Landsat ETM+ imagery: A case study in Phoenix, USA. *Int. J. Remote Sens.* **2007**, *28*, 269–291. [CrossRef]
57. Gu, Z.J.; Zeng, Z.Y. Overview of researches on vegetation coverage in remote sensing. *Res. Soil Water Conserv.* **2005**, *12*, 18–21.
58. Li, X.B.; Chen, Y.H.; Shi, P.J.; Chen, J. Detecting vegetation fractional coverage of typical steppe in northern china based on multi-scale remotely sensed data. *Acta Bot. Sin.* **2003**, *45*, 1146–1156.